Plasma Sci. Technol. **19** (2017) 025402 (9pp) doi:10.1088/2058-6272/19/2/025402

Evolution of plasma parameters in an Ar–N_2/He inductive plasma source with magnetic pole enhancement

Maria YOUNUS[1], N U REHMAN[2], M SHAFIQ[1], M NAEEM[1], M ZAKA-UL-ISLAM[3] and M ZAKAULLAH[1]

[1] Department of Physics, Plasma Physics Laboratory, Quaid-i-Azam University, 45320 Islamabad, Pakistan
[2] Plasma Physics Laboratory, Department of Physics, COMSATS Institute of Information Technology, 44000 Islamabad, Pakistan
[3] Department of Physics, Faculty of Science, Jazan University, 114 Jazan, Saudi Arabia

E-mail: najeeb-ur-rehman@comsats.edu.pk

Received 17 June 2016, revised 22 September 2016
Accepted for publication 23 September 2016
Published 3 January 2017

Abstract

Magnetic pole enhanced inductively coupled plasmas (MaPE-ICPs) are a promising source for plasma-based etching and have a wide range of material processing applications. In the present study Langmuir probe and optical emission spectroscopy were used to monitor the evolution of plasma parameters in a MaPE-ICP Ar–N_2/He mixture plasma. Electron density (n_e) and temperature (T_e), excitation temperature (T_{exc}), plasma potential (V_p), skin depth (δ) and the evolution of the electron energy probability function (EEPF) are reported as a function of radiofrequency (RF) power, pressure and argon concentration in the mixture. It is observed that n_e increases while T_e decreases with increase in RF power and argon concentration in the mixture. The emission intensity of the argon line at 750.4 nm is also used to monitor the variation of the 'high-energy tail' of the EEPF with RF power and gas pressure. The EEPF has a 'bi-Maxwellian' distribution at low RF powers and higher pressure in a pure N_2 discharge. However, it evolves into a 'Maxwellian' distribution at RF powers greater than 70 W for pure N_2, and at 50 W for higher argon concentrations in the mixture. The effect of argon concentration on the temperatures of two electron groups in the 'bi-Maxwellian' EEPF is examined. The temperature of the low-energy electron group T_L shows a decreasing trend with argon addition until the 'thermalization' of the two temperatures occurs, while the temperature of high-energy electrons T_H decreases continuously.

Keywords: MaPE-ICP, Langmuir probe, OES, EEPF

(Some figures may appear in colour only in the online journal)

1. Introduction

Low-pressure inductively coupled plasmas (ICPs) are widely used in material processing (e.g. surface coatings and dry etching in the semiconductor industry). ICPs have advantages over other plasma sources due to high plasma densities, homogeneous spatial profiles of reactive species, low plasma sheath potentials and an independently controllable ion energy. The magnetic pole enhanced ICP (MaPE-ICP) sources offer some extra features, such as high electron density, better power coupling efficiency, large area compatibility and low electron temperature [1]. Like conventional ICPs, MaPE-ICPs operate in two modes, the E and H modes, the properties of which are significantly different. In the E mode the discharge operates at a low power with low excitation efficiency, lower electron density and elevated electron temperature. In contrast, the H mode is characterized by high excitation efficiency, low electron temperature and higher electron density ($\sim 10^{11}$ cm^{-3}) [2, 3].

Pure nitrogen and its mixture discharges are extensively used for material processing [4, 5]. The addition of an inert gas like argon, helium or neon in a nitrogen plasma leads to an enhancement of reactive species of nitrogen due to Penning excitation and ionization processes. Moreover, the electron temperature can be 'tuned' by the addition of inert gases to a nitrogen plasma [6]. Therefore, to understand the kinetics of the discharges accurate knowledge of electron number density and temperature, as well as the electron energy distribution function (EEDF), is required. In molecular gases like nitrogen, vibrational and rotational excitations play a key role in the evolution of the EEDF [7]. In low-temperature non-local thermodynamic equilibrium plasma, a 'bi-Maxwellian' EEPF is usually present, and consequently such plasmas can be characterized by two distinct temperatures [8, 9].

The evolution of different plasma parameters and EEPFs in two operational modes of MaPE-ICP has not been reported extensively. Godyak *et al* [10] discussed variations in plasma parameters and power coupling efficiency using an ICP in conjunction with a ferromagnetic core. Jan *et al* [11] investigated a MaPE inductively coupled nitrogen–argon mixture plasma using a radiofrequency (RF)-compensated Langmuir probe. The increase in electron density was reported with the increase in argon concentration in the mixture. Jan *et al* [12] also investigated the evolution of the EEPFs for E and H modes in pure argon. Khan *et al* [13] reported the electron temperature and excitation temperature in a pure argon MaPE-ICP in which T_{exc} was validated as an alternative to T_e that is measured by a Langmuir probe.

The aim of the present study is to optimize a MaPE-ICP source for plasma-based surface treatment and etching by monitoring the evolution of various plasma parameters. In order to optimize the MaPE-ICP source, the variation in electron number density n_e, electron temperature T_e, excitation temperature T_{exc}, plasma potential V_p, skin depth δ and evolution of the EEPF in an Ar–N_2/He mixture plasma is monitored as a function of RF power, filling gas pressure and argon concentration in the discharge.

2. Experimental details

Figure 1 is a schematic diagram of the experimental setup. An RF-compensated Langmuir probe (Scientific Systems Smart Probe) is used to measure the plasma parameters, including n_e, T_e and V_p. The *I–V* characteristics and the EEDFs were also obtained by the probe. A tungsten wire 9.9 mm long and 0.2 mm in diameter is used as the probe tip. The *I–V* characteristic curves were interpreted using Smart Soft™ software (supplied by the manufacturer). The probe characteristics were analyzed by the software on the basis of the Laframboise orbital motion limited (OML) theory for a collisionless sheath. The Druyvesteyn method was used to obtain the EEDF from the second derivative of the probe current (d^2I/dU^2) as [14]

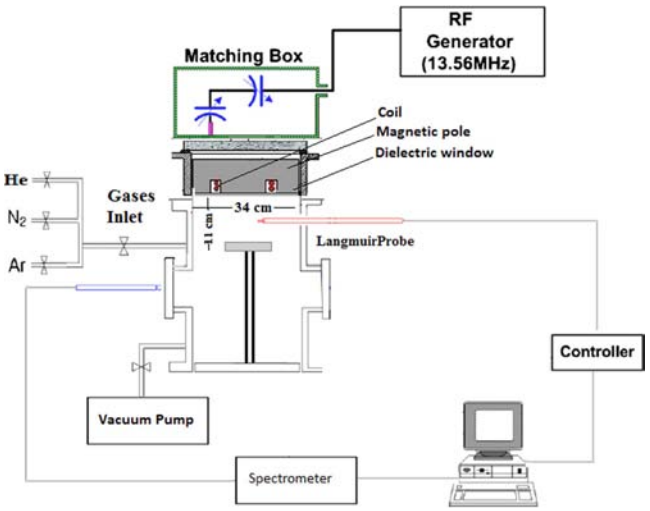

Figure 1. Schematic diagram of the experimental setup.

$$f(\varepsilon) = \frac{2\sqrt{2eUm_e}}{e^2 A_{lp}} \frac{d^2 I}{dU^2}. \quad (1)$$

Here I is the probe current, A_{lp} is the area of probe tip, m_e and e are the mass and charge of the electron, respectively, and $U (=V-V_p)$ is the probe potential with reference to V_p. V_p is measured at the zero crossing of the second derivative of I. The EEPF, $F(\varepsilon)$ is related to $f(\varepsilon)$ as

$$F(\varepsilon) = (\varepsilon)^{-1/2} f(\varepsilon). \quad (2)$$

n_e and T_e were obtained by integrating the EEDF as

$$n_e = \int_0^\infty f(\varepsilon) d\varepsilon$$
$$T_e = \frac{2}{3}\langle\varepsilon\rangle = \frac{2}{3n_e}\int_0^\infty \varepsilon f(\varepsilon) d\varepsilon. \quad (3)$$

A 13.56 MHz RF generator (PGF-RF Generator, 1600 W) coupled with a matching network (PFM 3000 A), powers the MaPE-ICP plasma source (a ferrite core MaPE-ICP 200, Fhr Anlagenbau Gmbh). The plasma was generated in a stainless steel chamber of height 25 cm and inner diameter 34 cm. A turbo molecular pump (Adixen ATP 200 T) backed by a rotary pump was used to maintain the pressure in the chamber and attain a base pressure of 0.0675 mTorr. The gas flow rate was controlled by Teledyne Hastings mass flow meters. The data were acquired at a fixed gas flow rate, i.e. 25 sccm. The argon/nitrogen concentrations were varied whereas the helium fraction was fixed at 4% throughout the experiment. The filling gas pressure was varied between 37.5 and 60 mTorr while RF power was varied from 20 to 300 W. The time-integrated emission spectra were recorded by an AVANTES (five-furcated) high-resolution spectrometer of spectral range 250–900 nm and then normalized for the spectral response of the fiber optics and optical window.

Table 1. Data used to calculate T_{exc} from selected Ar–I spectral lines [18].

λ_{ki} (nm)	E_k (eV)	g_k	A_{ki} (s^{-1})
687.12	14.71	3	2.78E + 06
696.54	13.32	3	6.39E + 06
737.21	14.75	9	1.90E + 06
738.39	13.30	5	8.47E + 06
750.38	13.47	1	4.45E + 07
751.46	13.27	1	4.02E + 07
800.61	13.17	5	4.90E + 06
811.53	13.07	7	3.31E + 07
842.46	13.09	5	2.15E + 07

3. Optical emission spectroscopy

Optical emission spectroscopy (OES) is a non-intrusive plasma diagnostic technique that is widely used for characterization of plasma parameters such as n_e, T_e, EEDF and T_{exc} [15, 16]. In the present study, OES is employed to determine T_{exc} using the Boltzmann plot technique. In this technique, intensities of selected spectral lines are used to determine T_{exc}. It is assumed that the selected excited states populate according to the Boltzmann distribution. Ar–I spectral lines that have approximately the same lower energy level, are used to measure the excitation temperature from the inverse of the slope of the Boltzmann plot [17]

$$\ln\left(\frac{I_{ki}\lambda_{ki}}{A_{ki}g_k}\right) = -\frac{E_k}{k_B T_{exc}} + C, \tag{4}$$

where λ_{ki} is the wavelength of spectral line, A_{ki} is the transition probability from level k to i, k_B is the Boltzmann constant, g_k is the statistical weight of excited level and C is a constant. The spectroscopic data required to evaluate the excitation temperature from equation (4) are given in table 1 [18].

4. Results and discussion

4.1. Electron density and temperature

To control the production and destruction rate of 'active species' due to electron impact, an accurate knowledge of n_e and temperature is required. Figures 2(a) and (b) show the variation in n_e (obtained with a Langmuir probe) with RF power and argon concentration in the Ar–N_2/He mixture at 37.5 and 60 mTorr, respectively. The results show that n_e increases with RF power and argon concentration in the mixture. This can be explained as follows. With an increase in RF power, the electrons gain more energy from the RF field and are able to cause further excitations and ionizations, resulting in an increase in n_e. Furthermore, it can be seen from the figure that required RF power for operating the discharge in H mode shifts towards a higher value with increasing nitrogen concentration in the mixture, i.e. for pure N_2 it is 50 W. This may be explained as follows: for higher nitrogen concentrations in the discharge, energy losses due to vibrational, rotational and dissociative excitation increase, therefore more power is required to sustain the H mode in the discharge [19]. Moreover, the electron collision cross section is greater for N_2 than argon in 1–10 eV energy range. Quenching of nitrogen excited states occurs and thus more RF power is required to sustain the discharge. Figure 2(b) shows an increase in n_e with an increase in argon concentration. The increase in n_e can be related to the decrease in electron mobility because it is inversely proportional to n_e. This decrease in mobility with increase in argon concentration causes thermalization of the discharge, which is also evident from figure 9. Moreover, the E–H mode transition with varying argon concentration in the mixture is also evident from figure 2(b). It is clear from the figure that at lower power (50 W) n_e increases considerably above 66% argon in the mixture, but as the RF power increases, the discharge remains in the H mode and the increase in the n_e is not significant. Figure 2(c) shows variation in n_e with filling gas pressure at a fixed RF power of 100 W for various argon concentrations in the mixture. It is clear from the figure that n_e decreases with an increase in pressure for different argon concentrations, but this trend changes for 86%Ar–10%N_2/4% He; i.e. n_e tends to increase with increasing pressure. As stated earlier, at higher argon concentrations in the mixture, electron–neutral scattering increases due to the lower collision cross section of argon compared with N_2 [20, 21]. On the other hand, at lower argon concentrations, the decrease in n_e with pressure is due to the higher electron collision cross section of N_2 as the electrons collide more frequently with N_2 molecules, hence only ro-vibrational excitations occur in the discharge. Moreover, with an increase in pressure the mean free path of electrons becomes smaller; they are not able to gain enough energy from the field between collisions. As a result excitation mechanisms dominate over ionization, and n_e decreases.

Figure 3(a) illustrates the variation in T_e (measured by Langmuir probe) with argon concentration at fixed RF powers (50 and 100 W) and a gas pressure of 60 mTorr. As shown in the figure, T_e decreases with argon concentration. Furthermore, the decrease becomes pronounced after addition of 66% argon at 50 W and after addition of 36% argon in the mixture at 100 W. This trend is understood in terms of inverse behavior of density and temperature. Moreover, the depletion of the high-energy electrons in the 'tail' of the EEDF at higher argon concentrations justifies the decreasing trend in T_e [22]. Figure 3(b) shows the variation in T_e with filling gas pressure for a fixed RF power of 100 W for different argon concentrations. It is evident from the figure that T_e initially increases with gas pressure for pure nitrogen and a low argon concentration in the mixture. But a decrease in T_e is observed for argon concentrations in the mixture of 76% and above. This can be understood in terms of the previously discussed trend of n_e with gas pressure. Further, it is also noted that T_e decreases with increase in RF power. This is due to the increase in electron–electron collision frequency with increase in RF power [11]. Figure 3(c) shows a comparison of the variation in the experimentally measured plasma parameters (n_e and T_e) in the present work and relevant data from the literature [23] that is closest to our experimental

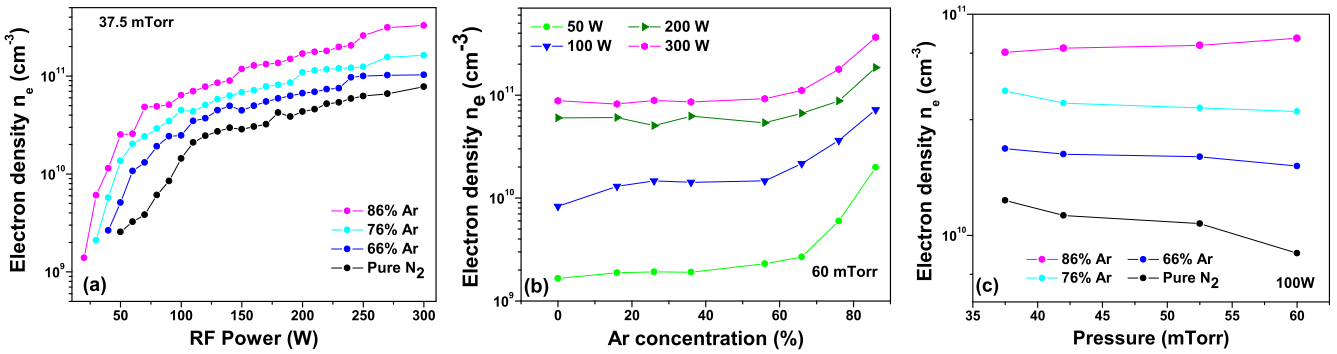

Figure 2. Variation in n_e with (a) RF power, (b) Ar concentration, and (c) pressure.

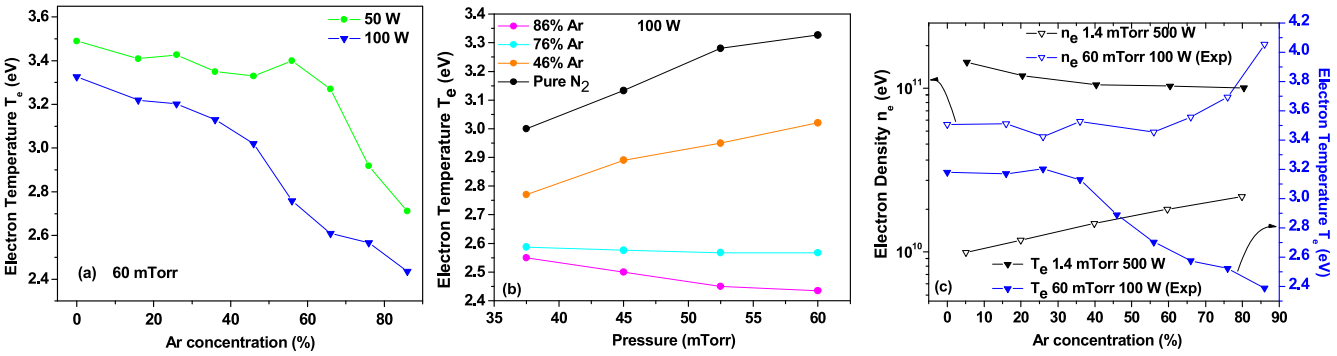

Figure 3. Variation of T_e (measured by a Langmuir probe) with (a) Ar concentration, (b) pressure and (c) comparison of the variation in n_e and T_e with the experimental results of Song *et al* [23].

conditions, to highlight the effect of magnetic pole enhancement of the ICP source. It can be ascertained from the figure that increased n_e and lower T_e are attributable to increased 'confinement' of the electrons in the discharge center owing to the presence of a ferrite core.

However, it is worth mentioning here that the *I–V* characteristic curves were interpreted using the software (Smart Soft^{TM}) supplied by the manufacturer, which analyzes the probe characteristics by using the Laframboise OML theory for a collisionless sheath. Thus, n_e (plasma density) has been obtained from the ion saturation current, which is not altered much in the presence of a magnetic field due to the larger Larmor radius of the ions. Moreover, in the presence of low to moderate fields, the electron currents are not varied much if the Langmuir probe is inserted perpendicular to the direction of the magnetic field [24], which is the case here. Furthermore, in the presence of magnetic field B the electron and ions in the plasma start orbiting around the magnetic field lines, with a radius equal to the Larmor radius. Generally, the Larmor radius of ions r_{Li} is greater than the dimension of the probe; hence the ion saturation current remains unaffected by the B field. On the other hand, the electron saturation current is reduced if it is measured along the field lines. However, the electron saturation current when measured with the probe set normal to the B field is not affected greatly. So it can be assumed that the B field does not greatly affect the probe current and the validity of the plasma parameters holds well [24].

4.2. Excitation temperature and emission intensity

T_e can be related to the 'excitation temperature' (T_{exc}) of the bound electrons in atoms or molecules because these excitation processes are initiated mostly by the free electrons [24]. In this way T_{exc} can serve as an alternative to T_e measured by the Langmuir probe. Figure 4(a) shows the variation in T_{exc} with argon concentration at fixed RF powers (50 and 100 W) and a pressure of 60 mTorr. The decrease in T_{exc} with argon concentration can be related to an increase in n_e at higher argon concentrations.

Figure 4(b) shows the variation in T_{exc} with gas pressure at fixed RF powers (50 and 100 W) and a 66% Ar concentration in the mixture. The decrease in T_{exc} can be understood in terms of the decrease in the 'mean free path' of electrons and the higher electron collision frequency with increase in gas pressure. Consequently, the electrons possess less energy at higher pressure and T_{exc} decreases. Furthermore, a 'platform' is noted in T_e measured by the Langmuir probe in the low Ar concentration region and not observed in T_{exc}. This can be explained as follows: Langmuir probe measurements of T_e are based on low-energy/bulk electrons while excitation temperature measured by the Boltzmann plot method is determined by the high-energy electrons.

The variation in electron density and excitation temperature, which indicates depletion of the high-energy tail, can also be described in terms of variation of emission intensity of the selected argon lines. Two argon lines at 750.4 nm ($2p_1 \rightarrow 1s_2$; $E_{th} = 13.48$ eV) (E_{th} is the minimum energy

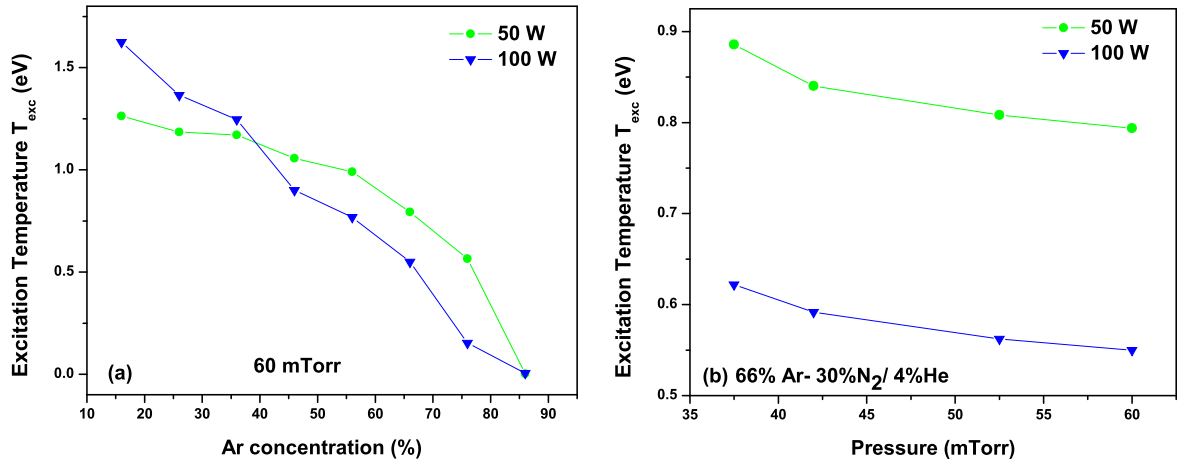

Figure 4. Behavior of T_{exc} with (a) Ar concentration and (b) pressure.

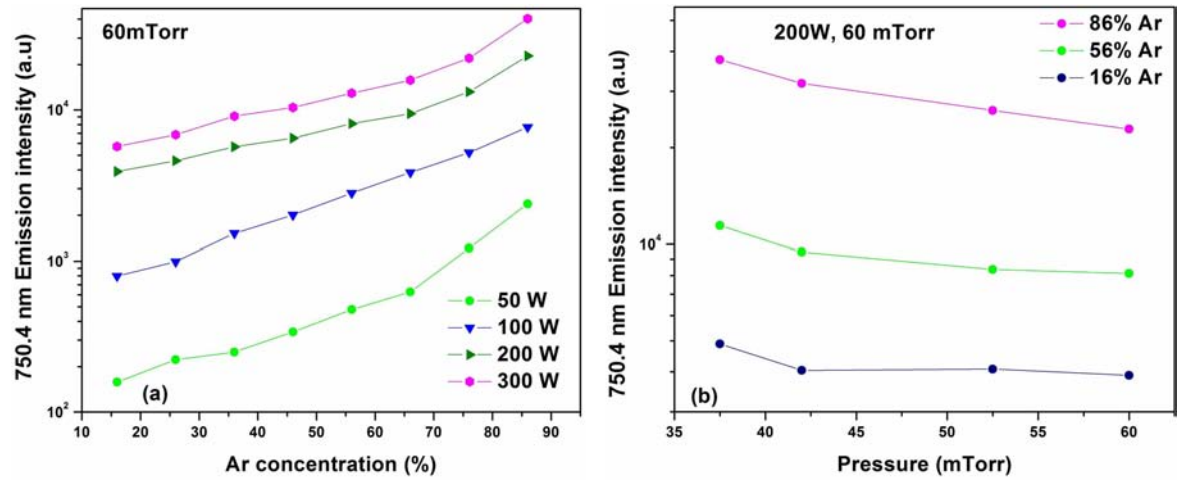

Figure 5. Variation in Ar 750.4 nm line emission intensity with (a) Ar concentration and (b) pressure.

required to reach the excited level to carry out the said transition) and 811.5 nm ($2p_9 \rightarrow 1s_5$; $E_{th} = 13.08$ eV) have been selected to observe the relation between electron density and emission intensity. By monitoring the excitation of these lines, as a function of discharge parameters, one can estimate the variation in n_e and T_e. Moreover, the variation in the line intensity ratio $I_{811.5}/I_{750.4}$ can also be used to describe the evolution in the EEPF, which is strongly linked with the changes in argon metastable state density [25]. Figure 5(a) shows the variation in the emission intensity of the 750.4 nm spectral line with argon concentration at different RF powers and a fixed pressure of 60 mTorr. It is clear from the figure that the emission intensity of the 750.4 nm line increases with argon concentration in the mixture and RF power. This increase confirms the presence of a large number of electrons having energy greater than the threshold energy of the 750.4 nm line. On the other hand, figure 5(b) shows a decreasing trend in the emission intensity of the argon 750.4 nm line with gas pressure at given RF power and argon concentration. This decrease can be attributed to variation in T_e with pressure, as discussed earlier.

Figure 6(a) shows the variation in the emission intensity of argon lines at 750.4 nm and 811.5 nm as a function of argon concentration at a fixed RF power of 300 W and gas pressure of 60 mTorr. The figure shows that the emission intensity of both spectral lines increases with argon addition. However, after reaching 56% argon in the mixture this increasing trend is reversed, i.e. the emission intensity of the 811.5 nm line increases more than the emission intensity of the 750.4 nm line. This result indicates that after 56% argon, the density of high-energy electrons starts to decrease in the discharge since the $2p_9$ state is strongly coupled with the metastable state $1s_5$. Figures 6(b) and (c) show the variation in intensity ratio $I_{811.5}/I_{750.4}$ with argon concentration and gas pressure, respectively. The increase in the $I_{811.5}/I_{750.4}$ ratio with argon concentration can be related to the decrease in emission intensity of the 750.4 nm line. This suggests a decrease in density of the available 'hot'/energetic electrons in the discharge due to their 'consumption' in intense ionization, leading to an increase in n_e. This is the main cause of the decreasing trend in T_e at higher argon concentrations.

4.3. Plasma potential and skin depth

The study of variation in V_p is important because its modification determines the strength of the electric field that

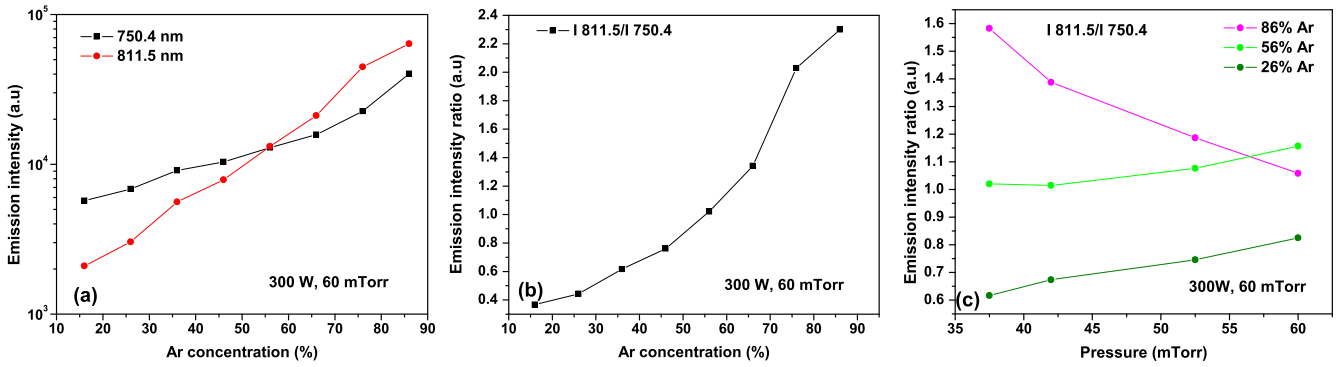

Figure 6. (a) Variation in Ar 750.4 nm and 811.5 nm line emission intensities with Ar concentration. Dependence of $I_{811.5}/I_{750.4}$ on (b) Ar concentration and (c) pressure.

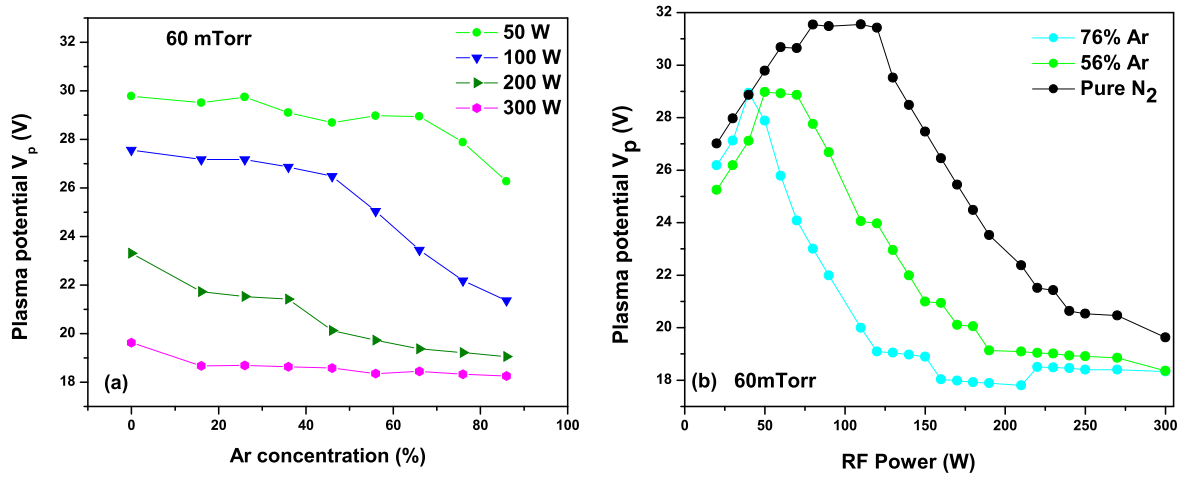

Figure 7. Variation in V_p with (a) Ar concentration and (b) RF power.

energizes the electrons to sustain the discharge through ionization. Figure 7(a) shows the variation in V_p with argon concentration in the mixture at various RF powers and a gas pressure of 60 mTorr. It is observed that V_p decreases as argon is added to the mixture. This suggests an increase in n_e in the discharge with argon concentration. Likewise, the variation of V_p with RF power is shown in figure 7(b). This figure shows that initially V_p increases with RF power, indicating a low degree of ionization. However, with a further increase in RF power V_p starts to decrease, which indicates that there is a considerable increase in the ionization rate, leading to increase in n_e, as shown in figure 2(a). It can also be seen from the figure that an increase in nitrogen concentration in the mixture leads to an elevated V_p. This may happen because of large total scattering cross section Q_T (1–10 eV) of nitrogen compared with argon [20, 21]. As a result, at higher N_2 concentrations in the discharge, more electrons tend to leave the plasma bulk and move towards the chamber walls. It is also noted that V_p increases with increase in filling gas pressure, but this effect becomes more prominent in mixtures in which nitrogen concentration increases.

Skin depth is the distance to which electromagnetic radiation can penetrate inside the plasma. Hence, it governs the spread of the electromagnetic field and also the mechanism of 'collisionless heating' of electrons and absorption of delivered RF power by the plasma. The collisionless skin depth, δ, is given by

$$\delta = \left(\frac{m}{e^2\mu_0 n_e}\right)^{1/2}, \tag{5}$$

where μ_0 is the permeability of free space. In this experiment, it is observed that n_e increases with argon concentration in the mixture. According to equation 5, this increase accompanies a decrease in δ, as shown in figure 8(a).

The 'analytical condition' for a steady H mode at low pressure is that δ must be smaller than the 'critical dimension' given by $(2/3)^{0.5}R$. Here R is the chamber dimension [26]. In the present study, the value of the critical dimension for a steady H mode is found to be 13.8 cm. It can be seen in figure 8(b), that variations in δ at different argon concentrations are prominent between 20 and 50 W.

At the beginning δ is greater than 13.8 cm, suggesting a deep electromagnetic field penetration into the plasma. At the E–H transition, it reduces to values less than the calculated critical dimension for the present experiment. In figure 8 it can also be seen that the calculated δ decreases with increasing RF power due to increase in n_e. In the present experiment, an interesting result regarding the variation of δ in pure nitrogen discharge is noted, i.e. during the E mode, the calculated δ is less than the value of the critical dimension.

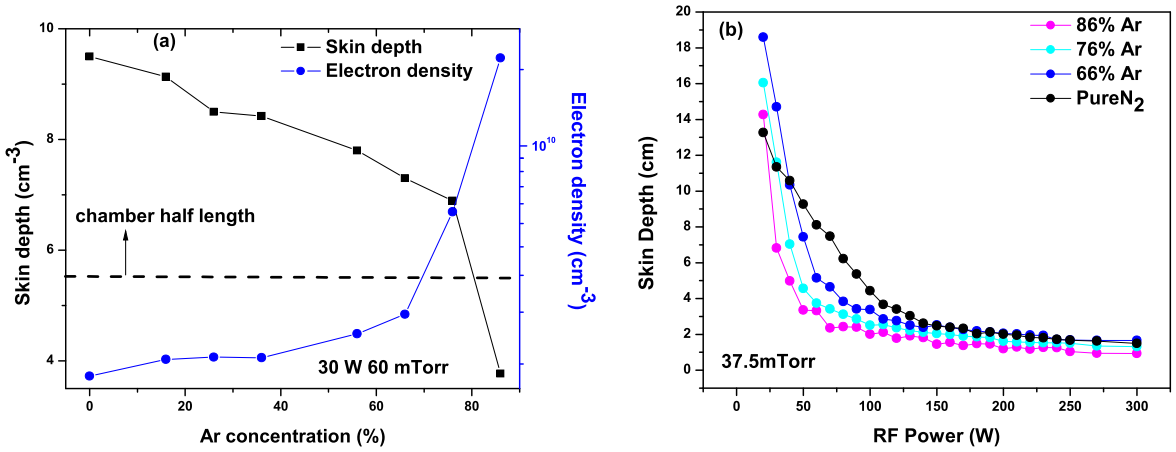

Figure 8. Variation in skin depth δ with (a) Ar concentration and (b) RF power.

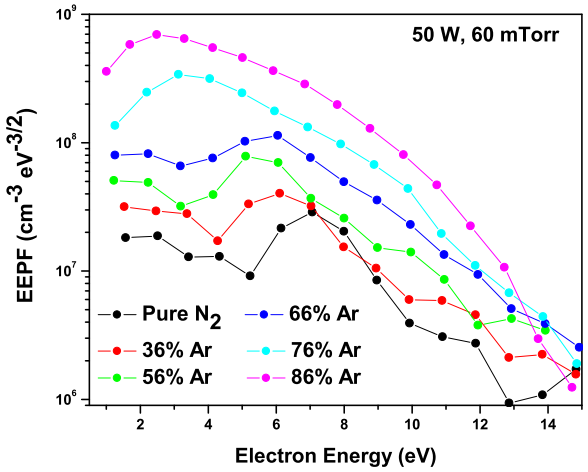

Figure 9. Evolution of EEPFs at various Ar concentrations at fixed RF power and pressure.

This is due to significant rotational excitation collisions between electrons and molecules in the E mode and is clear in figure 8(b).

4.4. Evolution of the EEPF profile

Figure 9 shows the evolution of EEPF profiles with argon concentration in the mixture at a fixed pressure of 60 mTorr and RF power of 50 W. It is evident from the figure that in a pure N_2 discharge the EEPF has a bi-Maxwellian distribution due to non-local electron kinetics at low gas pressures and RF powers [27]. The bi-Maxwellian EEPF in pure N_2 results from the collisionless heating of electrons due to the deep penetration of electromagnetic fields into the plasma, as is clear from figures 8(a) and (b).

A larger value of δ implies that the electrons have acquired sufficient energy and are able to surmount the ambipolar potential. However, the electrons that participate in vibrational/rotational excitations remain trapped in the potential well due to their low energies. That is why a dip appears in the EEPF profile at the resonant vibrational excitations. However, with an increase in argon concentration in the discharge (i.e. 76%), the EEPFs evolve into the Maxwellian distribution. This transformation of the EEPF profiles with increase in argon concentration in the gas mixture is related to modifications in the transport mechanisms in the plasma. As a result, n_e increases, which further enhances the electron–neutral collision/scattering frequency leading to collisional or Ohmic heating of low-energy electrons. Therefore, an evolution of EEPFs from a bi-Maxwellian to a Maxwellian distribution is noted, even at low gas pressure.

Figures 10(a) and (b) show the evolution of the EEPFs in pure N_2 and 76%Ar–20%N_2/4%He discharges at 60 mTorr for various RF powers. It is clear from the figure that EEPFs evolve from a bi-Maxwellian to a Maxwellian distribution with an increase in RF power, for both pure N_2 and for argon-added mixture discharges. The 'Maxwellization' of the electron distribution occurs due to an increase in n_e with RF power. This starts the redistribution of electron energy and thus EEPFs evolve from a bi-Maxwellian to a Maxwellian distribution with increase in RF power. On the other hand, the bi-Maxwellian nature of EEPF at low powers ($\leqslant$80 W for pure N_2 and $\leqslant$40 W for a 76% Ar mixture) can also be linked to variation in skin depth with RF power.

It is clear from figures 8(a) and (b) that at low RF powers δ is much greater than 5.5 cm, which is the chamber 'half length' from the substrate in the present case. This deep penetration of the RF field into the plasma bulk results in the collisionless heating of the electrons at the plasma center, and therefore the creation of two distinct groups of electrons occurs, i.e. bulk or low-energy electrons with temperature T_L and tail or high-energy electrons with temperature T_H. These temperatures are described by the bi-Maxwellian distribution function as [27]

$$f_e(\varepsilon) = A\left[\alpha \exp\left(\frac{-\varepsilon}{T_L}\right) + (1-\alpha)\exp\left(\frac{-\varepsilon}{T_H}\right)\right], \qquad (6)$$

where A is the normalization constant and $\alpha = (n_1/n_2)$ is ratio of the population of bulk electrons n_1 to the total number of electrons n_2. Figure 11 shows the variation, at different T_e, with argon concentration in the discharge at an RF power of 50 W and gas pressure 60 mTorr. It is illustrated in the figure that the temperature of high-energy electrons T_H decreases, which happens more drastically above 66% argon in the

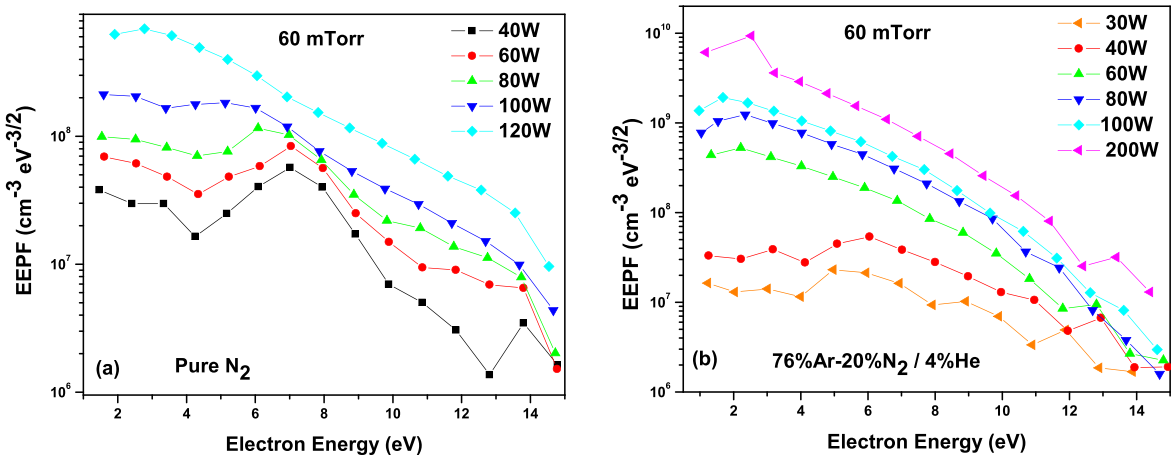

Figure 10. Evolution of EEPFs with RF power at fixed pressure: (a) pure N_2, (b) 76%Ar–20%N_2/4%He.

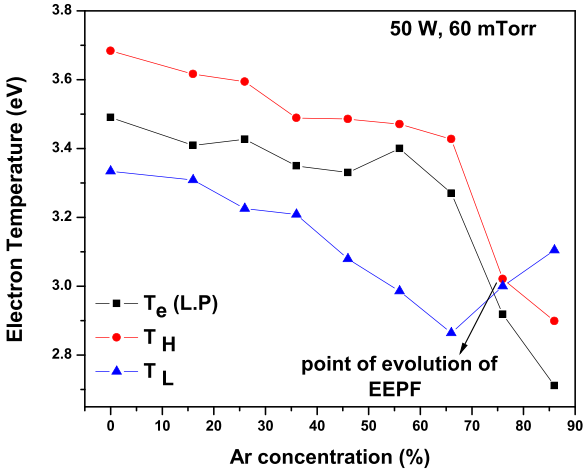

Figure 11. Variation in electron temperature T_e with Ar concentration at fixed pressure and RF power. T_e (L.P) is measured with a Langmuir probe, while T_H and T_L are calculated theoretically.

mixture. This decrease in temperature of high-energy electrons T_H can be explained in terms of the 'depletion' of the tail electrons in the EEPF [22]. This depletion arises due to the utilization of the high-energy electrons in the ionization process and, therefore, a steeper slope of the tail region in the EEPF profiles is observed in figure 9. The increase in ionization can also be related to the collisionless electron heating taking place in the plasma bulk due to deep penetration of electromagnetic fields into the bulk plasma. It is clear from figure 8(a) that δ remains greater than 5.5 cm, the chamber half length (from the substrate) in the present case, even at 76% argon in the mixture. Consequently, the low-energy electrons which remain limited to the 'ambipolar potential well' are able to move into the skin layer and get heated effectively. These electrons, upon colliding with neutrals, cause increased ionization. At the same time, generation of 'cold electrons' via the ionization process leads to an increase in bulk electron density, which decreases the bulk electron temperature T_L. It is also noted that T_L starts to increase at 66% or argon in the mixture and above. This may be due to collisional heating of bulk plasma electrons due to increase in electron–neutral scattering. This trend of T_e is found to be opposite to that in a He–N_2/Ar discharge [28].

5. Conclusions

In this paper, the influence of RF power, gas pressure and argon concentration on plasma parameters including n_e, T_e, T_{exc}, V_p, δ and the EEPF is investigated in a MaPE-ICP Ar–N_2/He mixture plasma. The results show that n_e has an increasing trend with RF power and argon concentration in the mixture, whereas T_e has a decreasing trend. It is noted that at 86% argon in the discharge, n_e increases with pressure instead of decreasing while T_e also shows the inverse behavior. Furthermore, plasma potential increases and decreases with low and high RF power, respectively. It is also found that δ decreases with RF power, indicating an increase in n_e. At low RF powers (<50 W) in a pure N_2 discharge, the EEPF has a bi-Maxwellian distribution, which evolves into a Maxwellian distribution with an increase in argon concentration. T_{exc} and the temperature of high-energy electrons (T_H) decrease with argon addition. Similarly, the low-energy electron temperature (T_L) decreases with the argon percentage; however, it increases beyond the point of 'thermalization' of the temperatures.

Acknowledgments

This study was aided by the Higher Education Commission (HEC) under the NRPU Research Project no. 2997/R & D/14 COMSATS Institute of Information Technology and also HEC Research Project no. 20-2002 (R&D) Quaid-i-Azam University. Maria Younus is grateful to Z. Anjum of CIIT for her help. We are grateful to the referee(s) for the valuable suggestions for improvement of the manuscript.

References

[1] Meziani T, Colpo P and Rossi F 2001 *Plasma Source. Sci. Technol.* **10** 276
[2] Kortshagen U, Gibson N D and Lawler J E 1996 *J. Phys. D: Appl. Phys.* **29** 1224
[3] Turner M M and Lieberman M A 1999 *Plasma Source. Sci. Technol.* **8** 313
[4] Kimura T and Kasugai H 2010 *J. Appl. Phys.* **108** 033305
[5] Czerwiec T, Greer F and Graves D B 2005 *J. Phys. D: Appl. Phys.* **38** 4278
[6] Bai K H *et al* 2002 *Phys. Plasmas* **9** 2831
[7] Britun N *et al* 2007 *J. Phys. D: Appl. Phys.* **40** 1022
[8] Godyak V A, Piejak R B and Alexanderovich B M 1993 *J. Appl. Phys.* **73** 3657
[9] Seo S H *et al* 2000 *Appl. Phys. Lett.* **76** 149
[10] Godyak V A 2011 *Plasma Source. Sci. Technol.* **20** 025004
[11] Jan F *et al* 2012 *J. Appl. Phys.* **112** 063305
[12] Jan F *et al* 2012 *Eur. Phys. J.* D **66** 103
[13] Khan A W *et al* 2012 *Curr. Appl. Phys.* **13** 1241
[14] Druyvesteyn M J 1930 *Z. Phys.* **64** 781
[15] Behringer K and Fantz U 1994 *J. Phys. D: Appl. Phys.* **27** 2128
[16] Donnelly V M 2004 *J. Phys. D: Appl. Phys.* **37** R217
[17] Park H and Choe W 2010 *Curr. Appl. Phys.* **10** 1456
[18] http://physics.nist.gov/cgi-bin/ASD
[19] Lee Y W, Lee H L and Chung T H 2011 *J. Appl. Phys.* **109** 113302
[20] Raju G G 2006 *IEEE Electr. Insul. Mag.* **22** 5
[21] Itikawa Y 2006 *J. Phys. Chem. Ref. Data* **35** 31
[22] Kang Z D and Pu Y K 2002 *Chin. Phys. Lett.* **19** 1139
[23] Song M A, Lee Y W and Chung T H 2011 *Phys. Plasmas* **18** 023504
[24] Grill A 1994 *Cold Plasma in Materials Fabrication: From Fundamentals to Applications* (New Jersey: IEEE Press)
[25] Czerwiec T and Graves D B 2004 *J. Phys. D: Appl. Phys.* **37** 2827
[26] Lee M H and Chung C W 2006 *Phys. Plasmas* **13** 063510
[27] Godyak V A, Meytlis V P and Strauss H R 1995 *IEEE Trans. Plasma Sci.* **23** 728
[28] Younus M *et al* 2016 *Phys. Plasmas* **23** 023512